Spin-orbital entangled molecular j_{eff} states in lacunar spinel compounds

Heung-Sik Kim[1], Jino Im[2], Myung Joon Han[1,3] & Hosub Jin[4,5]

The entanglement of the spin and orbital degrees of freedom through the spin-orbit coupling has been actively studied in condensed matter physics. In several iridium oxide systems, the spin-orbital entangled state, identified by the effective angular momentum j_{eff}, can host novel quantum phases. Here we show that a series of lacunar spinel compounds, GaM_4X_8 (M = Nb, Mo, Ta and W and X = S, Se and Te), gives rise to a molecular j_{eff} state as a new spin-orbital composite on which the low-energy effective Hamiltonian is based. A wide range of electron correlations is accessible by tuning the bandwidth under external and/or chemical pressure, enabling us to investigate the cooperation between spin-orbit coupling and electron correlations. As illustrative examples, a two-dimensional topological insulating phase and an anisotropic spin Hamiltonian are investigated in the weak and strong coupling regimes, respectively. Our finding can provide an ideal platform for exploring j_{eff} physics and the resulting emergent phenomena.

[1] Department of Physics, Korean Advanced Institute of Science and Technology, Daejun 305-701, Korea. [2] Department of Physics and Astronomy, Northwestern University, Evanston, Illinois 60208, USA. [3] KAIST Institute for the NanoCentury, Korean Advanced Institute of Science and Technology, Daejun 305-701, Korea. [4] Center for Correlated Electron Systems, Institute for Basic Science (IBS), Seoul 151-747, Korea. [5] Department of Physics and Astronomy, Seoul National University, Seoul 151-747, Korea. Correspondence and requests for materials should be addressed to H.J. (email: jinhs76@snu.ac.kr).

S pin-orbit coupling (SOC) is a manifestation of Einstein's theory of relativity in condensed matter systems. Recently, SOC has attracted a great deal of attention since it is a main ingredient for spintronics applications[1,2], induces novel quantum phases[3,4] and generates new particles and elementary excitations[5,6]. Moreover, when incorporated with electron correlations, SOC can give rise to even more fascinating phenomena[7,8]. In the iridium oxide family, where the IrO_6 octahedron is the essential building block, various quantum phases have been predicted or verified according to the electron correlation strength on top of the large SOC of the Ir $5d$ t_{2g} orbital: topological band insulator for weak coupling[9,10], Weyl semi-metal, axion insulator, non-Fermi liquid and TI* phases for intermediate coupling[11–15], and topological Mott insulator and quantum spin liquid phases for strong coupling[7,16,17].

Emergence of the spin-orbital entangled j_{eff} states induced by SOC[18,19] is the key feature to host all the above phases, yet the existence of such states is limited to a small number of iridate compounds only. Here, the series of lacunar spinel compounds[20,21], GaM_4X_8, where early $4d$ or $5d$ transition metal atoms occupy the M-site, are found to provide the molecular form of the j_{eff} basis in their low-energy electronic structures. The idealness of the molecular j_{eff} state is guaranteed by the formation of the M_4 metal cluster and the large SOC. Combined with the ability to control the electron correlation from the weak to strong coupling limit, the lacunar spinels can manifest themselves as the best candidates to demonstrate this so-called j_{eff} physics.

Results

Formation of the molecular j_{eff} states in $GaTa_4Se_8$. The chemical formula and crystal structure of the GaM_4X_8 lacunar spinels are easily deduced from the spinel with half-deficient Ga atoms, that is, $Ga_{0.5}M_2X_4$. Due to the half removal of the Ga atoms, the transition metal atoms are strongly distorted into the tetrahedral center as denoted by the red arrows in Fig. 1a, and a tetramerized M_4 cluster appears. The M_4 cluster yields a short intra-cluster M–M distance, naturally inducing the molecular states residing on the cluster as basic building blocks for the low-energy electronic structure. On the other hand, the large inter-cluster distance results in a weak inter-cluster bonding and a narrow bandwidth of the molecular states.

As a representative example of the lacunar spinels, we investigate the electronic structure of $GaTa_4Se_8$ (Fig. 1b–d). Figure 1b shows the band structure and the projected density of states (PDOS) of $GaTa_4Se_8$ in the absence of SOC. In consistency with previous studies[21–23], the triply degenerate molecular t_2 bands occupied by one electron are located near the Fermi level with a small bandwidth of ∼0.75 eV. As shown in the PDOS plot, the molecular t_2 bands are dominated by Ta t_{2g} orbital components; the small admixture of Se $5p$ and the strong tetramerization imply that the molecular t_2 states consist of direct bonding between Ta t_{2g} states.

The molecular nature of the low-energy electronic structure can be visualized by adopting the maximally localized Wannier function scheme[24,25]. The three molecular t_2 Wannier functions depicted in Fig. 1c read

$$| D_\alpha \rangle = \frac{1}{2} \sum_{i=1}^{4} | d_\alpha^i \rangle \quad (\alpha = xy, yz, zx), \qquad (1)$$

where D_α and d_α denote the molecular t_2 and atomic t_{2g} states, respectively, and i is a site index indicating the four corners of the M_4 cluster. Each D_α originates from a σ-type strong bonding between the constituent t_{2g} orbitals in the M_4 cluster. (See Supplementary Note 1, Supplementary Fig. 1 and Supplementary

Table 1 for details on the molecular t_2 Hamiltonian.) Owing to the exact correspondence between the molecular t_2 and the atomic t_{2g} states, as revealed in equation 1, the molecular t_2 triplet carries the same effective orbital angular momentum $l_{eff} = 1$ as the atomic t_{2g} orbital[18]. By virtue of SOC, the $l_{eff} = 1$ states are entangled with the $s = 1/2$ spin, and two multiplets designated by the effective total angular momentum $j_{eff} = 1/2$ and $3/2$ emerge. The band structure and PDOS of $GaTa_4Se_8$ in the presence of SOC verify the above j_{eff} picture (Fig. 1d); the molecular t_2 bands split into upper $j_{eff} = 1/2$ and lower $j_{eff} = 3/2$ bands. The separation between the two j_{eff} subbands is almost perfect owing to the large SOC of the Ta atoms as well as the small bandwidth of the molecular t_2 band. An alternative confirmation of the j_{eff} picture can also be given by constructing the Wannier function from each of the j_{eff} subbands, which shows a 99% agreement with the ideal molecular j_{eff} states. (See Supplementary Fig. 2.) Consequently, the electronic structure of $GaTa_4Se_8$ can be labelled as a quarter-filled $j_{eff} = 3/2$ system on a face-centered cubic lattice.

Robust j_{eff}-ness in the GaM_4X_8 series. The aforementioned j_{eff}-ness in $GaTa_4Se_8$ remains robust in the GaM_4X_8 series with a neighbouring $5d$ transition metal (M = W) as well as the $4d$ counterparts (M = Nb and Mo). Among the series, M = W compounds have not been reported previously in experiments; thus we use optimized lattice parameters by structural relaxations. In Fig. 2a–d, the electronic structures of $GaTa_4Se_4Te_4$[26], $GaW_4Se_4Te_4$, $GaNb_4Se_8$[21] and $GaMo_4Se_8$[27] are shown—band structure, PDOS and Fermi surface with projection onto the molecular j_{eff} states. In Fig. 2a,b, one can see the clear separation and identification of the higher $j_{eff} = 1/2$ doublet and the lower $j_{eff} = 3/2$ quartet driven by the large SOC of the $5d$ transition metal atoms. The overall band dispersions are quite similar, except for the location of the Fermi level; the M = Ta and M = W lacunar spinels are well characterized by the quarter-filled $j_{eff} = 3/2$ and the half-filled $j_{eff} = 1/2$ systems, respectively. In $4d$ compounds, the separation between the j_{eff} subbands is reduced due to the smaller SOC compared with that of the $5d$ systems (Fig. 2c,d). Nevertheless, there is a discernible splitting between the $j_{eff} = 1/2$ and $3/2$ bands, which is comparable to or even better than that in the prototype j_{eff} compounds, Sr_2IrO_4 and Ba_2IrO_4[28].

To acquire a well-identified j_{eff} band, we need the j_{eff} state as a local basis, and the inter-orbital hopping terms between the j_{eff} subspaces should be suppressed. Hence, there are three important conditions to realize the ideal j_{eff} system: high symmetry protecting the $l_{eff} = 1$ threefold orbital degeneracy, small bandwidth minimizing the inter-orbital mixing and large SOC fully entangling the spin and orbital degrees of freedom. The lacunar spinel compounds comfortably satisfy the above conditions; the tetrahedral symmetry of the M_4 cluster protects the orbital degeneracy, the long inter-cluster distance leads to the small bandwidth and a large SOC is inherent in $4d$ and $5d$ transition metal atoms.

Figure 2e introduces one important controlling parameter—the bandwidth. By changing the inter-cluster distance via external pressure and/or by substituting chalcogen atoms, the bandwidth of the molecular t_2 band can be tuned over a wide range. In the M = Ta series, for example, the bandwidth varies from 0.4 to 1.1 eV. Consequently, the effective electron correlation strength, given by the ratio between the bandwidth and the on-site Coulomb interactions, can be controlled to reach from the weak to the strong coupling regime. In fact, the bandwidth-controlled insulator-to-metal transitions were observed in $GaTa_4Se_4$ and $GaNb_4Se_4$[23,29], implying that both the weakly and strongly interacting limits are accessible in a single compound.
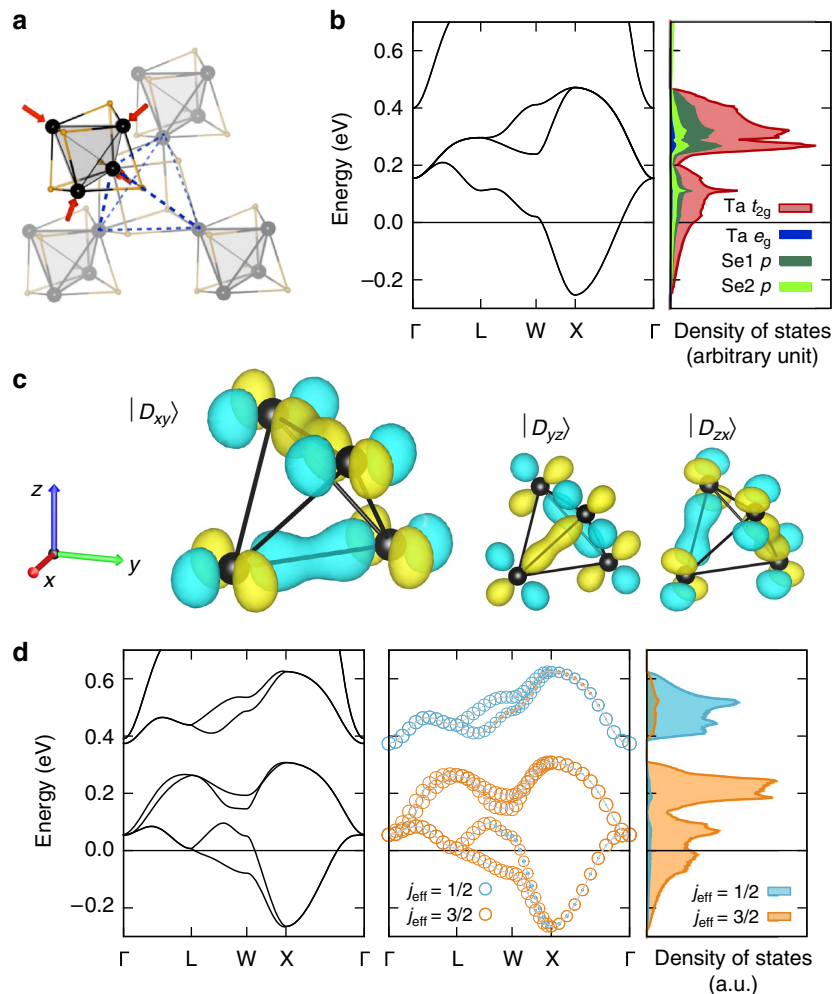
Figure 1 | Molecular form of spin–orbital entangled j_{eff} states in GaTa$_4$Se$_8$. (**a**) The connectivity between the neighbouring M$_4$ clusters and the local distortion of each cluster. (**b**) Band structure and PDOS of GaTa$_4$Se$_8$ without SOC. (**c**) Three Wannier orbitals constructed from the triplet molecular orbital bands near the Fermi level. (**d**) Band structure and DOS with SOC, projected onto the $j_{eff} = 1/2$ and 3/2 subspaces. The size of the circle in the band structure shows the weight of each subspace in each Bloch state.

Effective Hamiltonian. From the apparent separation between the j_{eff} subbands, as well as the similar band dispersions, the GaM$_4$X$_8$ series are governed by a common effective Hamiltonian composed of two independent $j_{eff} = 1/2$ and 3/2 subspaces, that is, $\mathcal{H}_{eff} \simeq \mathcal{H}^{1/2} \oplus \mathcal{H}^{3/2}$. (See Supplementary Notes 2 and 3.) Therefore, the compounds with M = Nb/Ta and M = Mo/W are described by the quarter-filled $\mathcal{H}^{3/2}$ and the half-filled $\mathcal{H}^{1/2}$ systems, respectively. The nearest-neighbor hopping terms for each subspace are written as

$$\mathcal{H}^{\tau}_{hopping} = \sum_{\langle ij \rangle} \mathbf{C}^{\dagger}_{i\tau} \mathbf{T}^{\tau}_{ij} \mathbf{C}_{j\tau} \quad (\tau = 1/2, 3/2), \quad (2)$$

with $\mathbf{T}^{1/2}_{ij} = t^0 \mathbf{I} + i \boldsymbol{t}^D_{ij} \cdot \mathbf{S}^{1/2}$

$\mathbf{T}^{3/2}_{ij} = t^0 \mathbf{I} + i \boldsymbol{t}^D_{ij} \cdot \mathbf{S}^{3/2} + \boldsymbol{t}^Q_{ij} \cdot \boldsymbol{\Gamma}$,

where $\mathbf{S}^{1/2}$ and $\mathbf{S}^{3/2}$ are the $j_{eff} = 1/2$ and 3/2 pseudospin matrices, respectively, and $\boldsymbol{\Gamma}$ are the 5-component Dirac Gamma matrices. t^0 and $\boldsymbol{t}^Q$'s are even, and $\boldsymbol{t}^D$'s are odd functions under the spatial inversion; $\boldsymbol{t}^D$'s are allowed by the inversion asymmetry of the M$_4$ cluster. The pseudospin-dependent hopping terms $\boldsymbol{t}^D$ and $\boldsymbol{t}^Q$ can

be interpreted as the effective magnetic dipolar and quadrupolar fields acting on the hopping electron, respectively.

DFT + SOC + U calculations. So far, we have discussed about the j_{eff}-ness without containing electron correlations, which provides a valid picture in the weak coupling regime. Once taking electron correlations into account, one important question arises on the robustness of the molecular j_{eff} states under the influence of the on-site Coulomb interaction. To answer this question, we perform DFT + SOC + U calculations for GaTa$_4$Se$_4$Te$_4$, GaW$_4$Se$_4$Te$_4$, GaNb$_4$Se$_8$ and GaMo$_4$Se$_8$. We consider two simplest magnetic configurations, ferromagnetic and antiferromagnetic order, and the antiferromagnetic solutions for each compound are shown in Fig. 3. In the 5d compounds, the molecular j_{eff} states remain robust with developing a SOC-assisted Mott gap within each j_{eff} subspace (Fig. 3a,b). For the 4d compounds, the j_{eff} character is enhanced from the non-interacting cases in Fig. 2c,d; the occupied states in GaNb$_4$Se$_8$ (Fig. 3c) and the unoccupied states in GaMo$_4$Se$_8$ (Fig. 3d) are dominated by $j_{eff} = 3/2$ and 1/2 characters, respectively. The strengthened j_{eff} character by the cooperation with electron correlations is consistent with the recent theoretical results on Sr$_2$IrO$_4$[28,30]. See the Supplementary
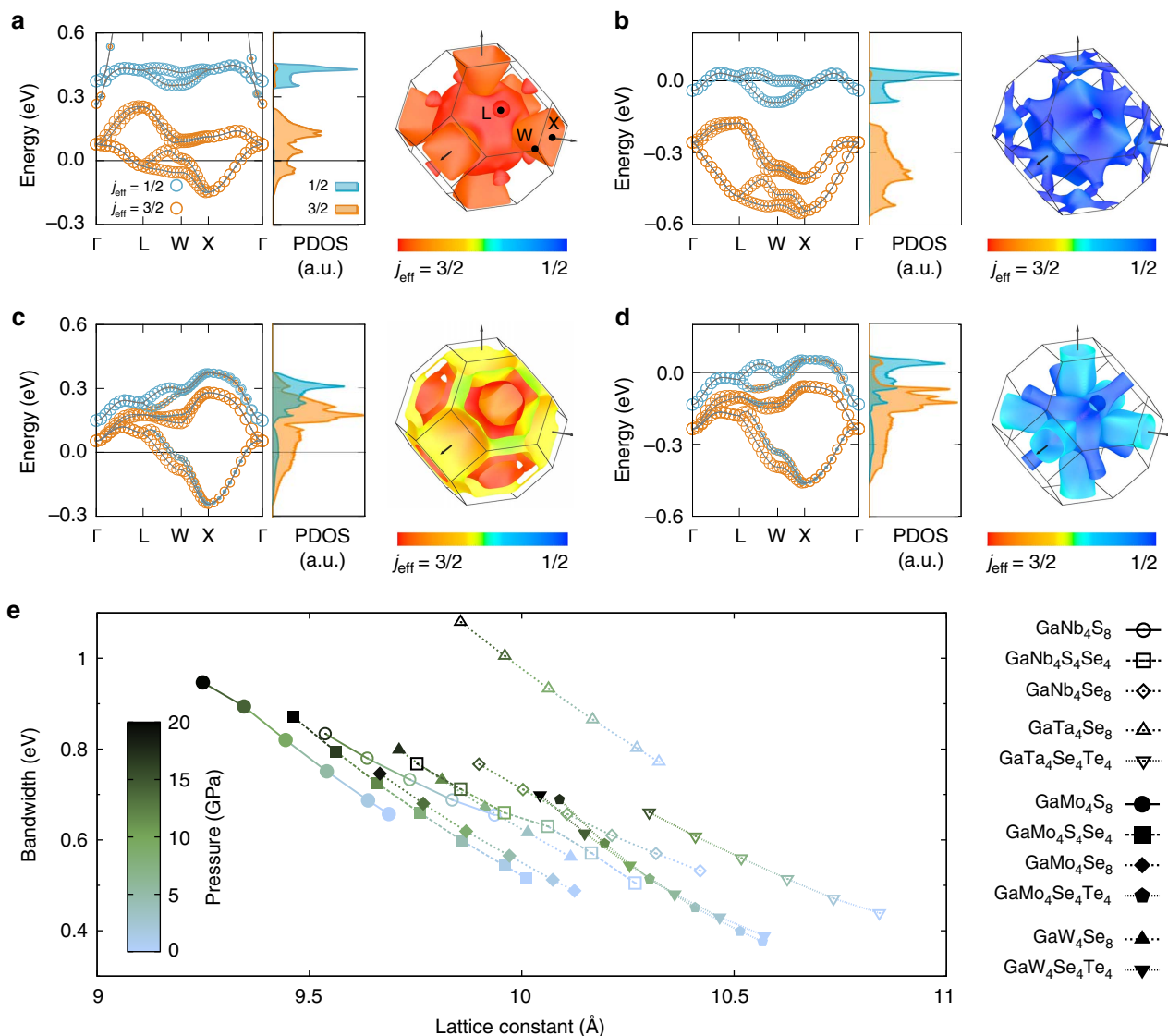
Figure 2 | j_{eff}-ness in the GaM$_4$X$_8$ series. The molecular j_{eff}-projected band structures, DOS and the Fermi surfaces of (**a**) GaTa$_4$Se$_4$Te$_4$, (**b**) GaW$_4$Se$_4$Te$_4$, (**c**) GaNb$_4$Se$_8$ and (**d**) GaMo$_4$Se$_8$ are presented. (**e**) The relation between the external hydrostatic pressure, lattice constant and bandwidth of the molecular t_2 bands in the absence of SOC.

Note 4, Supplementary Figs 3–6 and Supplementary Tables 2–5 for more details.

Discussion

The effective Hamiltonian of the lacunar spinel series has intriguing implications both in the weak and strong coupling regimes. As suggested in previous studies[3,9,31], the effective fields exerted on the hopping electron can induce a topological insulating phase in the weak coupling regime. In fact, a non-trivial band topology is realized within the molecular j_{eff} bands in thin film geometries: the monolayer (Fig. 4a) and the bilayer thin film (Fig. 4b) of the M$_4$ clusters normal to the (111) direction. Each system corresponds to the triangular and honeycomb lattice, respectively, and the inter-layer coupling enhanced by a factor of three is adopted in the bilayer system. Non-trivial gaps emerge in the half-filled $j_{eff}=3/2$ bands in the monolayer and the half-filled $j_{eff}=1/2$ bands in the bilayer system. A two-dimensional (2D) topological insulator phase is indicated by an odd number of edge Dirac cones at time-reversal invariant momenta in ribbon geometries (Fig. 4a,b). Such 2D geometries might be feasible with the help of the state-of-the-art epitaxial technique prevailing

in oxide perovskite compounds[32], or by mechanically cleaving the single crystal to get clean surfaces as done in previous studies on GaTa$_4$Se$_8$[33,34].

In the strong coupling regime, the large on-site Coulomb terms are added to the kinetic Hamiltonian, and the hopping terms $\mathbf{T}_{ij}^{\tau}$ are treated as perturbations. The localized j_{eff} pseudospins become low-energy degrees of freedom and exchange interactions between the neighbouring j_{eff} moments emerge. In the simplest example, the one-band Hubbard model within the half-filled $\mathcal{H}^{1/2}$, the resulting spin Hamiltonian for the $j_{eff}=1/2$ moments is written as[35,36]

$$\mathcal{H}_{spin}^{1/2} = \sum_{\langle ij \rangle} \left[\mathbf{J}\mathbf{s}_i \cdot \mathbf{s}_j + \mathbf{D}_{ij} \cdot \left(\mathbf{s}_i \times \mathbf{s}_j \right) + \mathbf{s}_i \cdot \mathbf{A}_{ij} \cdot \mathbf{s}_j \right], \quad (3)$$

among the exchange interaction terms, the Dzyaloshinskii–Moriya $\mathbf{D}_{ij}$ and the pseudodipolar interaction $\mathbf{A}_{ij}$ depend on t_{ij}^D, whose direction is determined by the two mirror planes, as illustrated in Fig. 4c (details in Supplementary Note 5). As shown in Fig. 4d, the relative magnitude of each exchange term is changed with different chalcogen atoms, so that systematic study of the anisotropic Hamiltonian in equation 3 can be made in the
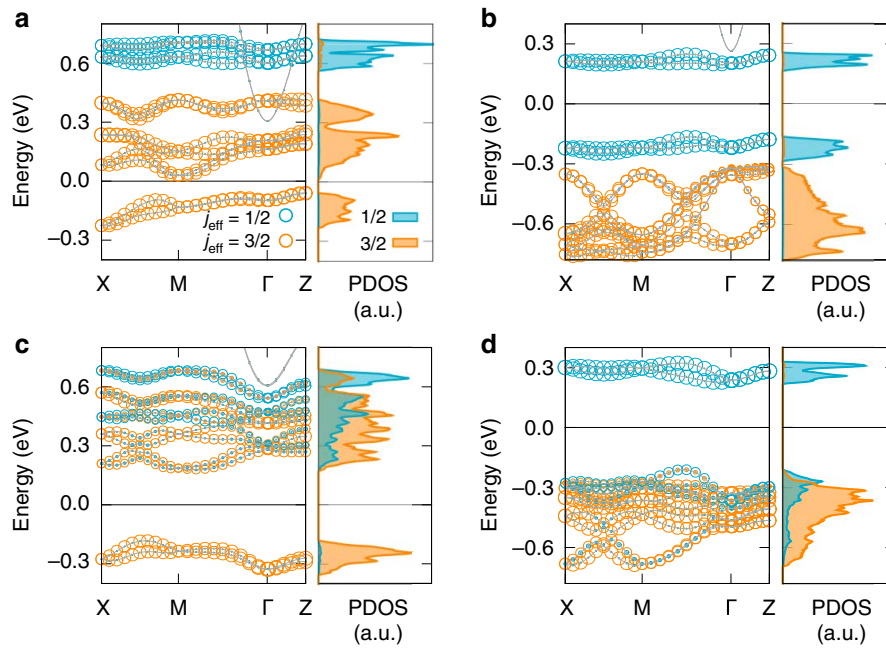
Figure 3 | DFT + SOC + U calculations. The j_{eff}-projected band structure and DOS of (**a**) GaTa$_4$Se$_4$Te$_4$, (**b**) GaW$_4$Se$_4$Te$_4$, (**c**) GaNb$_4$Se$_8$ and (**d**) GaMo$_4$Se$_8$ with the presence of electron correlations and antiferromagnetic order.
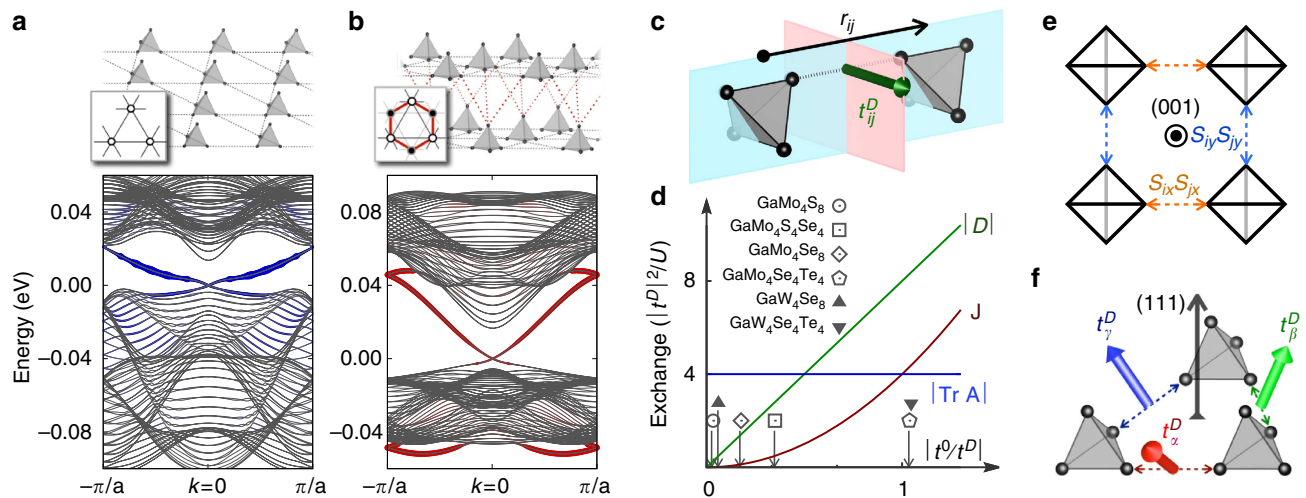
Figure 4 | Topological insulating phases and anisotropic spin model. The one-dimensional band structure of (**a**) half-filled $j_{eff} = 3/2$ monolayer and (**b**) half-filled $j_{eff} = 1/2$ bilayer M$_4$ ribbons (20 unit cell width). The insets show schematic top view of each system, where the thin grey and the thick red lines represent the intra- and the inter-planar bonding, respectively. The thickness of the coloured fat lines in the band structure represent the weights on the edge. (**c**) Two mirror planes (blue and red) existing in between the neighbouring M$_4$ clusters determine the direction of $\mathbf{t}_{ij}^D$ illustrated as green arrow. (**d**) Magnitudes of Heisenberg (dark red), Dzyaloshinskii–Moriya (green) and pseudodipolar (blue) exchange interactions as a function of $|t_0/\mathbf{t}^D|$. The magnitude of $|t_0/\mathbf{t}^D|$ for each of the M = Mo/W compounds is marked on the horizontal axis. (**e**) The 90°- and (**f**) the 60°-compass interactions are realized on (001) and (111) M$_4$ monolayers, respectively.

M = Mo/W compounds. Especially, GaMo$_4$S$_8$ and GaW$_4$Se$_8$ satisfies the limit of $|t_0/\mathbf{t}^D| \rightarrow 0$, where the spin Hamiltonian becomes highly anisotropic and bond direction dependent such that

$$\mathcal{H}_{spin}^{1/2} \rightarrow \sum_{\langle ij \rangle} \mathbf{s}_i \cdot \mathbf{A}_{ij} \cdot \mathbf{s}_j = \frac{4\,|t^D|^2}{U} \sum_{\langle ij \rangle} \left[2(\mathbf{s}_i \cdot \hat{\mathbf{t}}_{ij}^D)(\mathbf{s}_j \cdot \hat{\mathbf{t}}_{ij}^D) - \mathbf{s}_i \cdot \mathbf{s}_j \right],$$

(4)

with $\hat{\mathbf{t}}_{ij}^D = \mathbf{t}_{ij}^D / |\mathbf{t}^D|$. In addition to the Heisenberg term, the Hamiltonian contains the bond-dependent and Ising-like

pseudodipolar interaction, called as a Heisenberg-compass model[37]. It can be further reduced to distinct 2D spin models in thin-film geometries. Figure 4e,f shows two examples—the (001) and (111) monolayer lead to the 90°- and 60°-compass model with the Heisenberg exchange term on a square and a triangular lattice, respectively.

The $j_{eff} = 3/2$ systems in the strong coupling limit could also have a significant implication in terms of unconventional multipolar orders[38–40]. On top of the nonmagnetic insulating behaviour, the weak tetragonal superstructure and the anomalous magnetic response observed in GaNb$_4$S$_8$ at T $\sim$ 31 K[41] could give

some clues on the quadrupolar ordered phase as well as the spin liquid phase suggested in ref. 39, which promptly calls for further research on the $j_{eff} = 3/2$ spin model.

The formation of the M_4 cluster and SOC are the essential requisites to realize the molecular j_{eff} state in these 3D intermetallic compounds. The strong tetramerization sustains the isolated molecular bands with threefold orbital degeneracy and narrow bandwidth, and the large SOC fully entangles the spin and orbital components. The existence of the pure quantum state has been shedding light on studying the ideal quantum model systems in strongly correlated physics; the Hubbard Hamiltonian or the frustrated spin Hamiltonian based on the pure spin-half state has been realized in several organic compounds[42–44]. Likewise, the molecular form of the ideal j_{eff} state as a pure quantum state might be of great use to explore the emergent phenomena in the spin-orbit-coupled correlated electron systems.

Methods

First-principles calculations. Structural optimizations were done with the projector augmented wave potentials and the PBEsol[45] generalized gradient approximation as implemented in the Vienna *ab initio* Simulation Package[46,47]. Momentum space integrations were performed on a $12 \times 12 \times 12$ Monkhorst-Pack grid, and a 300-eV energy cutoff was used for the plane-wave basis set. The force criterion was 10^{-3} eV Å^{-1}, and the pressures exerted were estimated by using the Birch–Murnaghan fit.

For the electronic structure calculations, we used OPENMX code[48] based on the linear-combination-of-pseudo-atomic-orbital basis formalism. Four hundred Rydberg units of energy cutoff was used for the real-space integration. SOC was treated via a fully relativistic *j*-dependent pseudopotential in a non-collinear scheme. Simplified DFT + U formalism by Dudarev *et al.*[49], implemented in OPENMX code[50], was adopted in the DFT + SOC + U calculations. $U_{eff} \equiv U - J = 2.5$ and 2.0 eV was used for the $4d$ and $5d$ compounds, respectively.

References

1. Datta, S. & Das, B. Electronic analog of the eletro-optic modulator. *Appl. Phys. Lett.* **56**, 665–667 (1990).
2. Pesin, D. & MacDonald, A. H. Spintronics and pseudospintronics in graphene and topological insulators. *Nat. Mater.* **11**, 409–416 (2012).
3. Kane, C. L. & Mele, E. J. Quantum spin Hall effect in graphene. *Phys. Rev. Lett.* **95**, 226801 (2005).
4. Chang, C.-Z. *et al.* Experimental observation of the quantum anomalous Hall effect in a magnetic topological insulator. *Science* **340**, 167–170 (2013).
5. Qi, X.-L., Li, R., Zang, J. & Zhang, S.-C. Inducing a mangetic monopole with topological surface states. *Science* **323**, 1184–1187 (2009).
6. Fu, L. & Kane, C. L. Superconducting proximity effect and Majorana fermions at the surface of a topological insulator. *Phys. Rev. Lett.* **100**, 096407 (2008).
7. Pesin, D. & Balents, L. Mott physics and band topology in materials with strong spin-orbit interaction. *Nat. Phys.* **6**, 376–381 (2010).
8. Witczak-Krempa, W., Chen, G., Kim, Y. B. & Balents, L. Correlated quantum phenomena in the strong spin-orbit regime. *Annu. Rev. Condens. Matter Phys.* **5**, 57–82 (2014).
9. Shitade, A. *et al.* Quantum spin Hall effect in a transition metal oxide Na$_2$IrO$_3$. *Phys. Rev. Lett.* **102**, 256403 (2009).
10. Guo, H. M. & Franz, M. Three-dimensional topological insulators on the pyrochlore lattice. *Phys. Rev. Lett.* **103**, 206805 (2009).
11. Wan, X., Turner, A. M., Vishwanath, A. & Savrasov, S. Y. Topological semimetal and Fermi-arc surface states in the electronic structure of pyrochlore iridates. *Phys. Rev. B* **83**, 205101 (2011).
12. Go, A., Witczak-Krempa, W., Jeon, G. S., Park, K. & Kim, Y. B. Correlation effects on 3D topological phases: from bulk to boundary. *Phys. Rev. Lett.* **109**, 066401 (2012).
13. Wan, X., Vishwanath, A. & Savrasov, S. Y. Computational design of axion insulators based on 5d spinel compounds. *Phys. Rev. Lett.* **108**, 146601 (2012).
14. Moon, E.-G., Xu, C., Kim, Y. B. & Balents, L. Non-fermi-liquid and topological states with strong spin-orbit coupling. *Phys. Rev. Lett.* **111**, 206401 (2013).
15. Maciejko, J., Chua, V. & Fiete, G. A. Topological order in a correlated three-dimensional topological insulator. *Phys. Rev. Lett.* **112**, 016404 (2014).
16. Okamoto, Y., Nohara, M., Aruga-Katori, H. & Takagi, H. Spin-liquid state in the S = 1/2 hyperkagome antiferromagnet Na$_4$Ir$_3$O$_8$. *Phys. Rev. Lett.* **99**, 137207 (2007).
17. Chaloupka, J., Jackeli, G. & Khaliullin, G. Kitaev-Heisenberg model on a honeycomb lattice: possible exotic phases in iridium oxides A_2IrO$_3$. *Phys. Rev. Lett.* **105**, 027204 (2010).
18. Kim, B. J. *et al.* Novel J$_{eff}$ = 1/2 Mott state induced by relativistic spin-orbit coupling in Sr$_2$IrO$_4$. *Phys. Rev. Lett.* **101**, 076402 (2008).
19. Kim, B. J. *et al.* Phase-sensitive observation of a spin-orbital mott state in Sr$_2$IrO$_4$. *Science* **323**, 1329–1332 (2009).
20. Pocha, R., Johrendt, D. & Pöttgen, R. Electronic and structural instabilities in GaV$_4$S$_8$ and GaMo$_4$S$_8$. *Chem. Mater.* **12**, 2882–2887 (2000).
21. Pocha, R., Johrendt, D., Ni, B. & Abd-Elmeguid, M. M. Crystal structures, electronic properties, and pressure-induced superconductivity of the tetrahedral cluster compounds GaNb$_4$S$_8$, GaNb$_4$Se$_8$, and GaTa$_4$Se$_8$. *J. Am. Chem. Soc.* **127**, 8732–8740 (2005).
22. Camjayi, A., Weht, R. & Rozenberg, M. Localised Wannier orbital basis for the Mott insulators GaV$_4$S$_8$ and GaTa$_4$Se$_8$. *Europhys. Lett.* **100**, 57004 (2012).
23. Ta Phuoc, V. *et al.* Optical conductivity measurements of GaTa$_4$Se$_8$ under high pressure: evidence of a bandwidth-controlled insulator-to-metal Mott transition. *Phys. Rev. Lett.* **110**, 037401 (2013).
24. Mazari, N. & Vanderbilt, D. Maximally-localized generalized Wannier functions for composite energy bands. *Phys. Rev. B* **56**, 12847–12865 (1997).
25. Souza, I., Mazari, N. & Vanderbilt, D. Maximally-localized Wannier functions for entangled energy bands. *Phys. Rev. B* **65**, 035109 (2001).
26. Guiot, V., Janod, E., Corraze, B. & Cario, L. Control of the electronic properties and resistive switching in the new series of Mott insulators GaTa$_4$Se$_{8-y}$Te$_y$ ($0 \leq y \leq 6.5$). *Chem. Mater.* **23**, 2611–2618 (2011).
27. Francois, M. *et al.* Structural phase transition in GaMo$_4$S$_8$ and AlMo$_4$S$_8$ by X-ray powder diffraction. *Zeitschrift für Kristallographie* **200**, 47–55 (1992).
28. Arita, R., Kuneš, J., Kozhevnikov, A., Eguiluz, A. & Imada, M. *Ab initio* studies on the interplay between spin-orbit interaction and Coulomb correlation in Sr$_2$IrO$_4$ and Ba$_2$IrO$_4$. *Phys. Rev. Lett.* **108**, 086403 (2012).
29. Abd-Elmeguid, M. *et al.* Transition from Mott insulator to superconductor in GaNb$_4$Se$_8$ and GaTa$_4$Se$_8$ under high pressure. *Phys. Rev. Lett.* **93**, 126403 (2004).
30. Zhang, H., Haule, K. & Vanderbilt, D. Effective J = 1/2 insulating state in Ruddlesden-Popper iridates: an LDA + DMFT study. *Phys. Rev. Lett.* **111**, 246402 (2013).
31. Haldane, F. D. M. Model for a quantum Hall effect without Landau levels: condensed-matter realization of the 'parity anomaly'. *Phys. Rev. Lett.* **61**, 2015–2018 (1988).
32. Xiao, D., Zhu, W., Ran, Y., Nagaosa, N. & Okamoto, S. Interface engineering of quantum Hall effects in digital transition metal oxide heterostructures. *Nat. Commun.* **2**, 596 (2011).
33. Dubost, V. *et al.* Resistive switching at the nanoscale in the Mott insulator compound GaTa$_4$Se$_8$. *Nano Lett.* **13**, 3648–3653 (2013).
34. Dubost, V. *et al.* Electric-field-assisted nanostructuring of a Mott insulator. *Adv. Funct. Mater.* **19**, 2800–2804 (2009).
35. Micklitz, T. & Norman, M. R. Spin Hamiltonian of hyper-kagome Na$_4$Ir$_3$O$_8$. *Phys. Rev. B* **81**, 174417 (2010).
36. Jackeli, G. & Khaliullin, G. Mott insulators in the strong spin-orbit coupling limit: from Heisenberg to a quantum compass and Kitaev models. *Phys. Rev. Lett.* **102**, 017205 (2009).
37. Nussinov, Z. & van den Brink, J. Compass and Kitaev models—Theory and Physical Motivations. Preprint at http://arxiv.org/abs/1303.5922 (2013).
38. Jackeli, G. & Khaliullin, G. Magnetically hidden order of Kramers doublets in d^1 systems: Sr$_2$VO$_4$. *Phys. Rev. Lett.* **103**, 067205 (2009).
39. Chen, G., Pereira, R. & Balents, L. Exotic phases induced by strong spin-orbit coupling in ordered double perovskites. *Phys. Rev. B* **82**, 174440 (2010).
40. Pi, S.-T., Nanguneri, R. & Savrasov, S. Y. Calculation of multipolar exchange interactions in spin-orbital coupled systems. *Phys. Rev. Lett.* **112**, 077203 (2014).
41. Jakob, S. *et al.* Structural and magnetic transitions in the Mott insulator GaNb$_4$S$_8$. *J. Mater. Chem.* **17**, 3833–3838 (2007).
42. Yamashita, S. *et al.* Thermodynamic properties of a spin-1/2 spin-liquid state in a κ-type organic salt. *Nat. Phys.* **4**, 459–462 (2008).
43. Kagawa, F., Miyagawa, K. & Kanoda, K. Magnetic Mott criticality in a κ-type organic salt probed by NMR. *Nat. Phys.* **5**, 880–884 (2009).
44. Yamashita, M. *et al.* Highly mobile gapless excitations in a two-dimensional candidate quantum spin liquid. *Science* **328**, 1246–1248 (2010).
45. Perdew, J. P. *et al.* Restoring the density-gradient expansion for exchange in solids and surfaces. *Phys. Rev. Lett.* **100**, 136406 (2008).
46. Kresse, G. & Hafner, J. *Ab initio* molecular dynamics for liquid metals. *Phys. Rev. B* **47**, 558–561 (1993).
47. Kresse, G. & Furthmüller, J. Efficient iterative schemes for *ab initio* total-energy calculations using a plane-wave basis set. *Phys. Rev. B* **54**, 11169–11186 (1996).
48. Ozaki, T. Variationally optimized atomic orbitals for large-scale electronic structures. *Phys. Rev. B* **67**, 155108 (2003).
49. Dudarev, S., Botton, G., Savrasov, S., Humphreys, C. & Sutton, A. Electron-energy-loss spectra and the structural stability of nickel oxide:An LSDA + U study. *Phys. Rev. B* **57**, 1505–1509 (1998).
50. Han, M. J., Ozaki, T. & Yu, J. O(N) LDA + U electronic structure calculation method based on the nonorthogonal pseudoatomic orbital basis. *Phys. Rev. B* **73**, 045110 (2006).

Author contributions

H.-S.K. and J.I. performed DFT calculations and data analysis with assistance from M.J.H. and H.J. All authors contributed to the discussion and the writing of the paper. H.J. was responsible for the conception and the overall direction.

Additional information

Supplementary Information accompanies this paper at http://www.nature.com/naturecommunications

Competing financial interests: The authors declare no competing financial interests.

Reprints and permission information is available online at http://npg.nature.com/reprintsandpermissions/

How to cite this article: Kim, H.-S. *et al.* Spin-orbital entangled molecular j_{eff} states in lacunar spinel compounds. *Nat. Commun.* 5:3988 doi: 10.1038/ncomms4988 (2014).